Molecular-dynamic study of the molecular glass model for $Rb_{1-x}(ND_4)_xD_2PO_4$

Krzysztof Parlinski* and Hans Grimm
Institut für Festkörperforschung, Kernforschungsanlage Jülich, D-5170 Jülich, Federal Republic of Germany
(Received 25 October 1985)

A two-dimensional model with four protons and two effective rubidium or ammonium particles per unit cell has been studied by the molecular-dynamic method. The symmetry properties of the phase transitions of RbD_2PO_4 and $ND_4D_2PO_4$ are used as input data for the simulation. The mixed system shows a glassy behavior. The freezing temperature T_f has been found by studying the glass order parameter η_τ. T_f depends on the time over which η_τ has been averaged. The calculations showed that below T_f the mixed system can go to many local minima which differ by displacement patterns. With the use of the multiple molecular-dynamic method with time averages and configurational averages over local minima, the diffuse scattering function and the dynamical structure factor have been calculated. Diffuse streaks along the high-symmetry axes of the crystal have been found. The width of the diffuse streak and of the quasielastic scattering exhibit a change of slope as a function of temperature, in agreement with the neutron-experimental observations.

I. INTRODUCTION

A structural analogue of a magnetic spin glass is the mixed system of ferroelectric RbH_2PO_4 or RbD_2PO_4 (RDP) and antiferroelectric $NH_4H_2PO_4$ or $ND_4D_2PO_4$ (ADP).[1] The paraelectric phases of RDP and ADP are isostructural at ambient temperature, the lattice constants are almost the same, and the solid solution $Rb_{1-x}(NH_4)_xH_2PO_4$ or $Rb_{1-x}(ND_4)_xD_2PO_4$ (RADP) can be obtained over the whole range of concentration.[2] Upon lowering the temperature, the mixed crystal with $x<0.22$ becomes ferroelectric, while that with $x>0.75$ becomes antiferroelectric. In the intermediate range of concentrations $0.22<x<0.75$, RADP maintains the overall paraelectric tetragonal structure down to the lowest temperature,[1] but the features of freezing into a glass state are already evident at 110 K.[2-5] The RADP system has been studied by variety of methods, including dielectric,[2,4] optical,[6] NMR,[5] x-ray,[4,7] and neutron[8] measurements.

The diffraction data[4,7-9] are of special interest since they throw some light on the structure of glass. For RADP crystals with $x=0.35$, Courtens *et al.*[4] have observed broad diffuse satellites at wave vector $\mathbf{k}=(\mu,0,0)$, where $\mu=0.25a^*$. Cowley *et al.*[7] studied crystals with $x=0.49$ and found diffuse streaks close to $\mu=0.35a^*$. We have performed[8] neutron-scattering measurements on the deuterated crystal $Rb_{0.38}(ND_4)_{0.62}D_2PO_4$, finding diffuse streaks along $\langle 100\rangle$ directions peaked at a distance $\mu=0.35a^*$, from some Bragg reflections. We have also measured the temperature behavior of the wave-vector width and energy width of the diffuse streaks. The widths of both quantities remain constant up to about 110 K and then increase.

A number of theoretical works have been devoted to molecular glasses like $(KCN)_x(KBr)_{1-x}$.[10,11] The interest in RADP glass is also remarkable.[12-15] In this crystal, because of its complexity, usually only the proton subsystem is considered using the Slater model, the cluster approximation,[12,13] and the replica method.[15] In effect, the order parameter, freezing temperature, phase diagram, lattice constants, and dielectric susceptibility behaviors were described. So far, no attempt has been made to calculate the diffuse scattering and the dynamical structure factor for RADP.

In this paper we introduce a two-dimensional model of RADP and solve it, by using the molecular-dynamic method. The model consists of a proton subsystem with four protons in the unit cell and two additional particles per unit cell which model the combined properties of Rb and PO_4 or ND_4 and PO_4. For RDP or ADP crystals the model parameters are chosen such that the system shows a phase transition to the ferroelectric or antiferroelectric phases, respectively. Some model parameters in both crystals are different, and in the mixed crystal they are taken to be in agreement with a given distribution of Rb and ND_4 particles. That simple assumption leads to many features which are characteristic for glass behavior. Monte Carlo simulations[16] for model KH_2PO_4 and molecular-dynamic simulations for potassium cyanide-bromide mixtures[11] have been performed. In the latter only the time averages were calculated. We have found, however, that the calculation of a diffuse-scattering function and the dynamical structure factor below the freezing temperature of a glass needs to be averaged not only over time but also over configurations of many equivalent states. The finite system in the computer can model different regions of the sample, just by using different initial conditions which drive the glass model system into different local minima. This multiple molecular-dynamic procedure leads to the configurational average specified in Sec. V.

The "observation" time τ available in the computer simulation is only of order $10^4\tau_0$, where $\tau_0=2\pi/\omega_0$, and ω_0 is the characteristic mode frequency, which is not always sufficient for a good average. Within this range of time there exists a freezing temperature T_f, depending on τ such that the longest relaxation time, in a broad spec-

trum of the relaxation times, exceeds the observation time τ when the temperature drops below $T_f(\tau)$, i.e., the system is approximately nonergodic due to the "impatience of the experimenter."[17] During a scattering experiment such as neutron scattering, the neutrons are even more "impatient observers." The observation time τ is specified by the energy resolution $\Delta\omega$ of the instrument and is, at most, of order of $10^2\tau_0$. The neutron probes differently noncorrelated regions or states of the sample.

The outline of the paper is as follows. In Sec. II the symmetry changes of pure RDP and ADP are considered. The results have been used in Sec. III to derive the potential energy of the two-dimensional model of RDP and ADP, with full agreement with the symmetry elements of the three-dimensional crystal. In Sec. IV we present the modifications introduced for the glass model. The molecular-dynamic method and its peculiarities are outlined in Sec. V. As a check of the model, the order parameters of RDP and ADP are given in Sec. VI. In Sec. VII the results of the phase diagram, average potential energy, glass order parameter, diffuse-scattering function, and dynamical structure factor are reported. The glass order parameter strongly depends on the observation time or averaging time τ. Using different initial conditions, the glass system could arrive in different local minima with entirely different diffuse-scattering patterns. Such local minima possess different patterns of particle displacement, even if they have the same distribution of Rb and ND_4 particles. Below freezing temperature the dynamical structure factor is accompanied by an elastic peak. Due to configurational averages, the results for the diffuse-scattering function and dynamical structure factor agree with experimental observations, including the temperature behavior of the widths of the diffuse streak and quasielastic peak. Final remarks are made in Sec. VIII.

II. SYMMETRY REDUCTIONS IN THE PHASE TRANSITIONS OF RDP AND ADP

A. Rubidium dihydrogen phosphate

RDP exists in paraelectric, tetragonal form, with space group $I\bar{4}2d$ (D_{2d}^{12}) ($Z=2$).[18,19] Below 148 and 218 K for hydrogenated and deuterated compounds, respectively, the crystal goes to the orthorhombic phase, with space group $Fdd2$ (C_{2v}^{19}) ($Z=2$). The phase transition is driven by $B_2\equiv\Gamma_3$ irreducible representations[20,21] at the Brillouin-zone center, i.e.,

$$I\bar{4}2d(Z=2)\rightarrow(\mathbf{k}_\Gamma=(0,0,0),\ \Gamma_3\equiv B_2)\rightarrow Fdd2(Z=2)\ . \tag{2.1}$$

The phase transition is elastic and ferroelectric because the strain component V_{xy} and the spontaneous polarization along the z axis transform according to Γ_3. Two domains of the ferroelectric phase can exist. Except for the unit representation Γ_1, no secondary order parameters[22] are present; therefore the Landau free-energy expansion takes a simple form

$$F=a\rho^2+b\rho^4+c\xi^2+d\rho^2\xi+\cdots\ ,$$

where ρ and ξ are the order parameters for the Γ_3 and Γ_1 representations, respectively. The coupling constant d is small and, therefore, the phase transition remains second order.

B. Ammonium dihydrogen phosphate

The paraelectric phase of ADP belongs to the same space group $I\bar{4}2d$ as the rubidium compounds. The structures are similar, with the obvious difference being that rubidium is substituted for by ammonium. Below 150 and 237 K, respectively, the crystal becomes antiferroelectric and orthorhombic, with space group $P2_12_12_1$ (D_2^4) ($Z=4$). The phase transition is driven by the sum of two complex-conjugate irreducible representations Z_2+Z_3 from the high-symmetry point $Z=(2\pi/a_0,\ 0,0)$ of the Brillouin-zone surface,

$$I\bar{4}2d(Z=2)\rightarrow(\mathbf{k}_Z=(2\pi/a_0,0,0),\ Z_2+Z_3)\rightarrow P2_12_12_1(Z=4)\ . \tag{2.2}$$

Four domains of the antiferroelectric phase can occur. Since there exists an intermediate space group, namely

$$I\bar{4}2d(Z=2)\supset I2_12_12_1(Z=2)\supset Fdd2(Z=4)\ ,$$

the phase transition is accompanied by the secondary order parameter[22] of symmetry Γ_4. Γ_4 describes the crystal shear $V_{xx}-V_{yy}$. The relevant Landau free-energy expansion for the paraelectric-ferroelectric phase transition can be written as

$$F=a'\rho_2\rho_3+b'(\rho_2^4+\rho_3^4)+c'\rho_2^2\rho_3^2+d'(\rho_2\rho_3)^3+e'(\rho_2^4+\rho_3^4)\rho_2\rho_3+f'\xi^2+g'\rho_2\rho_3\xi+h'\eta^2+j'(\rho_2^2+\rho_3^2)\eta+\cdots\ , \tag{2.3}$$

where ρ_2, ρ_3, ξ, and η are the order parameters for the Z_2, Z_3, Γ_1, and Γ_4 irreducible representations, respectively. Large coupling between the Z_2+Z_3 and Γ_4 (large $|j'|$) leads to the first-order phase transition. Below, we disregard this coupling, allowing for the second-order phase transition.

III. MODEL OF RDP AND ADP CRYSTALS

Using a molecular-dynamic method, one is not able to simulate a three-dimensional crystal with 36 degrees of freedom per unit cell (if treating PO_4 and ND_4 as rigid bodies) nor able to provide a satisfactory average over concentration, classify the modes with a large number of the wave vectors, etc. Therefore, it is reasonable to study rather a simplified, two-dimensional model.

The two-dimensional model should properly describe the symmetry changes of paraelectric to ferroelectric and antiferroelectric phases and take explicitly into account the hydrogen bonds and the spontaneous polarization of the crystal. That means the selected degree of freedom must be able to form the Γ_3 and Z_2+Z_3 irreducible representations, Eqs. (2.1) and (2.2). Thus, the two-dimensional model consists of unit cells addressed i,j with six particles in each unit cell (Fig. 1): four protons

$\nu=1,2,3,4$ at positions $(\frac{1}{2}+U,-\frac{1}{4})$, $(\frac{1}{2}-U,\frac{1}{4})$, $(\frac{3}{4},U)$, and $(\frac{1}{4},-U)$, where $U=\frac{1}{7}$, and two particles $\nu=5,6$ at (0,0) and $(\frac{1}{2},0)$, representing combined PO_4 and Rb or PO_4 and ND_4 groups. Each particle has one degree of freedom which is a displacement $u_{i,j,\nu}$ from its average position $R_{i,j,\nu}$. The protons $\nu=1,2$ and $\nu=3,4$ can move only along y and x directions, respectively, in the model plane, and these are the directions of the hydrogen bonds, while the particles $\nu=5,6$ can move only along z, the direction normal to the model plane.

The potential energy is assumed to depend on displacements of all particles and external fields and is proposed in the form of an expansion,

$$V=V^{(2)}+V^{(3)}+V^{(4)}+V_{\text{ext}}+\cdots , \tag{3.1}$$

where

$$\begin{aligned}V^{(2)}=\tfrac{1}{2}\sum_{i,j}\{&(A^{(1)}_{i,j}u^2_{i,j,1}+A^{(2)}_{i,j}u^2_{i,j,2}+A^{(3)}_{i,j}u^2_{i,j,3}+A^{(4)}_{i,j}u^2_{i,j,4}+A^{(5)}_{i,j}u^2_{i,j,5}+A^{(6)}_{i,j}u^2_{i,j,6})\\&-2E(u_{i,j,5}u_{i,j,6}+u_{i,j,5}u_{i-1,j,6}+u_{i,j,5}u_{i,j-1,6}+u_{i,j,5}u_{i-1,j-1,6})\\&+2C[u_{i,j,5}(u_{i-1,j,1}-u_{i,j-1,2}+u_{i-1,j-1,3}-u_{i,j,4})+u_{i,j,6}(u_{i,j,1}-u_{i,j,2}+u_{i,j,3}-u_{i,j,4})]\\&+2[B_{i,j,6}(u_{i,j,1}u_{i,j,4}-u_{i,j,1}u_{i,j,3})+B_{i+1,j,5}(u_{i,j,1}u_{i+1,j,4}-u_{i,j,1}u_{i,j-1,3})\\&\quad+B_{i,j,6}(u_{i,j,2}u_{i,j,3}-u_{i,j,2}u_{i,j,4})+B_{i,j+1,5}(u_{i,j,2}u_{i-1,j,3}-u_{i,j,2}u_{i,j+1,4})]\\&+2(D_{i,j,6}u_{i,j,1}u_{i,j,2}+D_{i,j,5}u_{i,j,1}u_{i+1,j-1,2}+D_{i,j,6}u_{i,j,3}u_{i,j,4}+D_{i,j,5}u_{i-1,j-1,3}u_{i,j,4})\\&+2P(u_{i,j,1}u_{i+1,j,2}+u_{i,j,3}u_{i,j+1,4})\}\ ,\end{aligned} \tag{3.2}$$

$$V^{(3)}=\tfrac{1}{2}\sum_{i,j}2H[u_{i,j,5}(u^2_{i-1,j,1}+u^2_{i,j-1,2}-u^2_{i-1,j-1,3}-u^2_{i,j,4})-u_{i,j,6}(u^2_{i,j,1}+u^2_{i,j,2}-u^2_{i,j,3}-u^2_{i,j,4})]\ , \tag{3.3}$$

$$V^{(4)}=\tfrac{1}{2}\sum_{i,j}G(u^4_{i,j,1}+u^4_{i,j,2}+u^4_{i,j,3}+u^4_{i,j,4}+u^4_{i,j,5}+u^4_{i,j,6})]\ , \tag{3.4}$$

$$\begin{aligned}V_{\text{ext}}=&-E_{\text{Rb}}\sum_{i,j}(u_{i,j,1}-u_{i,j,2}+u_{i,j,3}-u_{i,j,4}+u_{i,j,5}+u_{i,j,6})+E_{\text{NDy}}\sum_{i,j}(-1)^{i+j}(u_{i,j,1}+u_{i,j,2})\\&+E_{\text{NDx}}\sum_{i,j}(-1)^{i+j}(u_{i,j,3}+u_{i,j,4})\ .\end{aligned} \tag{3.5}$$

Each term of the expansion has the same form as the term with corresponding components of the potential energy of the three-dimensional crystal of RDP or ADP, and therefore the expansion (3.1)–(3.5) is consistent with the symmetry elements of $I\bar{4}2d$ space group. The quadratic term of potential energy consists of the local potential and interaction with few neighbors, while the fourth-order term is restricted to the local terms only. The local term of $V^{(3)}$ is forbidden by symmetry. The interaction of the order parameters of the ferroelectric and antiferroelectric phases with the external E_{Rb} and staggered E_{NDx},E_{NDy} electric fields, respectively, are defined in V_{ext}.

The way of selecting the numerical values of the parameters relied on the following procedure. Translational symmetry of the crystal requires $A^{(\nu)}_{i,j}=A$, $B^{(\nu)}_{i,j}=B$, and $D^{(\nu)}_{i,j}=D$. Thus, by the transformation,

$$u_{i,j,\nu}=\sum_{k,s}e_\nu(k,s)\exp(2\pi ikR_{i,j,\nu})\eta_{k,s}\ , \tag{3.6}$$

where $k=(k_x,k_y)$ and $s=1,2,\ldots,6$, $e_\nu(k,s)$ is the polarization vector, and $\eta_{k,s}$ is the normal-mode amplitude, the quadratic form $V^{(2)}$ of the pure crystal can be converted into a diagonal form,

$$V^{(2)}=\tfrac{1}{2}\sum_{k,s}\omega^2_{k,s}\eta_{k,s}\eta^*_{k,s}\ . \tag{3.7}$$

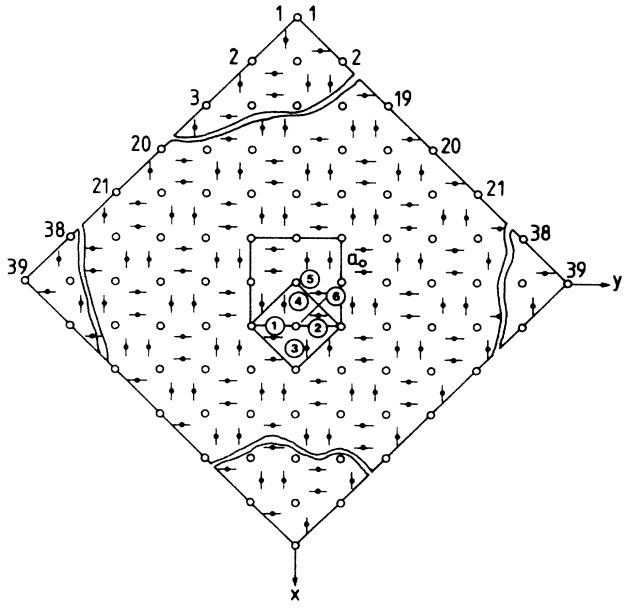

FIG. 1. Model system used in the molecular-dynamic simulation. The unit cell contains four protons, 1,2,3,4, and two combined Rb and PO_4 or ND_4 and PO_4 particles, 5,6. The direction of the hydrogen bounds are indicated. a_0 is the lattice constant of the tetragonal-body-centered unit cell.

TABLE I. Numerical values of potential-energy parameters for RDP and ADP models.

	Rb		ND_4		Rb	ND_4
A_{Rb}	−0.50	A_{ND}	−1.30	F	3.00	3.00
B_{Rb}	0.54	B_{ND}	0.20	P	0.80	0.80
C	0.50	C	0.50	H	3.00	3.00
D_{Rb}	−0.20	D_{ND}	−0.60	G	660.0	660.0
E	−0.50	E	−0.50			

In Fig. 2 the eigenvalues $\omega^2_{k,s}$ are drawn for two sets of parameters, given in Table I, one corresponding to the model of RDP, second to the model of ADP. They have been chosen according to the following conditions. In order to obtain the phase transition, the minimum values of $\omega^2_{k,s}$ must be negative. The absolute minimum of $\omega^2_{k,s}$ has to occur at $k=0$ for Γ_3 and at $k=(2\pi/a_0,0)$ for Z_2+Z_3 irreducible representations, for the RDP and ADP sets of parameters, respectively. The minima must be at the same level to ensure that both phase transitions occur at approximately the same temperature. The parameter A from $V^{(2)}$ must be negative and G from $V^{(4)}$ positive, so that they define local double minimum potential necessary to specify the hydrogen bound. The lowest branch should have a valley along Σ_2, i.e., the $\langle 10\rangle$ direction, in order to produce a diffuse streak there. A simple average $(1-x)\omega^{2(\mathrm{RDP})}_{k,s}+x\omega^{2(\mathrm{ADP})}_{k,s}$, where $0.3<x<0.7$ along Σ_2, should have a minimum for k values not at the $k=0$ or $k=(2\pi/a_0,0)$ points; otherwise the superlattice reflections will occur in the intermediate range of x and a pure glassy state would not be observed. It is obvious that an elaborate potential energy is needed to fulfill these requirements.

The local fourth-order term does not introduce any k dependence and the value of G is chosen so that the average low-temperature displacements are of the order $0.05a_0$. Then, the undesired multimode (similar to multiphonon) effects do not enter into the calculated structure factors.

Any branch of $\omega_{k,s}$ close to $k=0$ is isotropic. Consequently the valley along $\langle 10\rangle$ is shallow close to $k=0$ and can become deeper near the $k=(2\pi/a_0,0)$ point. For a good description of the experimental data, one would need a deep valley also close to the $k=0$ point. Only the introduction of an anisotropic acoustic mode could improve the situation, but then one needs a three-dimensional model with more degrees of freedom.

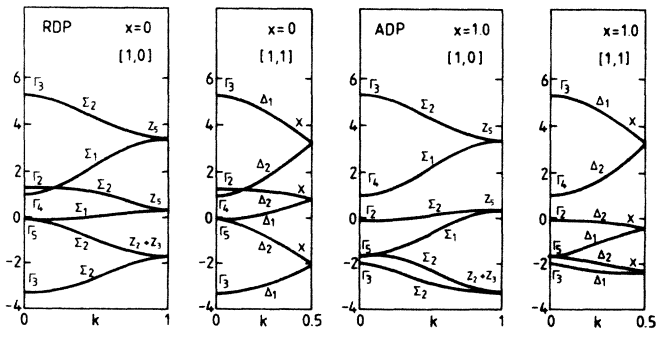

FIG. 2. Eigenvalues $\omega^2_{k,s}$ [Eq. (3.7)] of the quadratic part of the potential energy $V^{(2)}$, Eqs. (3.2), for RDP and ADP models, and for the parameters listed in Table I. $\omega_{k,s}$ is given in ω_0 units.

IV. MODEL OF A GLASS RADP

In the glass model the rubidium and ammonium particles are distributed randomly among $\nu=5,6$ sites, with a given concentration x. In such a mixture the potential energy (3.1)–(3.5) is no longer translationally invariant, and, therefore, the parameters of the i,j,ν particles in the potential energy are taken to be in agreement with the particles which occupy the neighboring $\nu=5,6$ sites, and the rules for that are as follows:

$$\begin{aligned} A_{i,j,\nu}&=A_{Rb}+(A_{ND}-A_{Rb})\delta_{i,j,\nu}\,,\\ B_{i,j,\nu}&=B_{Rb}+(B_{ND}-B_{Rb})\delta_{i,j,\nu}\,,\\ D_{i,j,\nu}&=D_{Rb}+(D_{ND}-D_{Rb})\delta_{i,j,\nu}\,, \end{aligned} \tag{4.1}$$

where $A_{Rb},\ldots,D_{ND}$ are given in Table I, and

$$\delta_{i,j,\nu}=\begin{cases}0 & \text{if in } (i,j,\nu) \text{ is Rb,}\\ 1 & \text{if in } (i,j,\nu) \text{ is } ND_4,\end{cases}$$

and the local potential parameters for protons are assumed to be an average of the appropriate A parameters for the nearest neighbors,

$$\begin{aligned} A^{(1)}_{i,j}&=\tfrac{1}{2}(A_{i+1,j,5}+A_{i,j,6})\,,\\ A^{(2)}_{i,j}&=\tfrac{1}{2}(A_{i,j+1,5}+A_{i,j,6})\,,\\ A^{(3)}_{i,j}&=\tfrac{1}{2}(A_{i+1,j+1,5}+A_{i,j,6})\,,\\ A^{(4)}_{i,j}&=\tfrac{1}{2}(A_{i,j,5}+A_{i,j,6})\,,\\ A^{(5)}_{i,j}&=A^{(6)}_{i,j}=F\,. \end{aligned} \tag{4.2}$$

V. MOLECULAR-DYNAMIC METHOD

The system used in the computer simulation was a square two-dimensional (2d) crystallite consisting of $N=38\times 38$ unit cells, Fig. 1. Two edges of the crystallite were supplemented with additional particles, $\nu=5$, so that along all edges only $\nu=5$ particles occur. In total, the system consisted of 8741 particles. Free-boundary conditions were used in order to allow extended defects, such as domain walls, to flow out of the system. The Newton equations of motion were solved by a simple difference

scheme using a vector computer (Cray). We used the microcanonical ensemble in which the total energy is conserved. The iteration step was $\Delta t = 0.05\tau_0$. The temperature was described by the average kinetic energy. The calculation started from initial conditions in the form of a random rectangular distribution for positions and velocities, and then the system was allowed to equilibrate. The system was heated or cooled by a delicate change (typically by a factor of 1.0005) of particle velocities in each iteration step.

We calculated two types of averages. The *time average* of a dynamical variable O, which was defined as

$$\langle O \rangle_\tau = \frac{1}{L} \sum_{l=1}^{L} O(l\,\Delta t) , \tag{5.1}$$

where $\tau = L\,\Delta t$ and L is the total number of iteration steps over which O was averaged. In a glassy state the simulated system can go to a local minimum, and in this state the time average alone may not produce representative results. The local minima, even for the same distribution of Rb and ND_4 particles, have generally different displacement patterns. The experimentally observed quantities are the averages over many local minimum states; therefore we have introduced the following *configurational average,*

$$\{\langle O \rangle_\tau\}_C = \frac{1}{C} \sum_{c=1}^{C} \langle O \rangle_\tau^{(c)} , \tag{5.2}$$

over C systems of 38×38 unit cells having the same concentration x and the same temperature, but calculated with different initial conditions. The concentration distribution can be the same or different. This approach can be called the multiple molecular-dynamic method. The configurational-averaging procedure is especially obvious for scattering methods such as neutron or light scattering in which each incident particle hits the crystal in another region and the regions can be quite independent. Moreover, the averaging time τ during which the system evolves, contributing to the configurational average (5.2), is straightforwardly related to the energy resolution $\Delta\omega$ of the method, since $\tau \sim 2\pi/\Delta\omega$.

We call the system approximately ergodic,[17] at least in the limits of time τ available in the computer simulation, if the time average over $C\tau$ is equal to the configurational average over short time τ,

$$\langle O \rangle_{C\tau} = \{\langle O \rangle_\tau\}_C ; \tag{5.3}$$

otherwise the system is called approximately nonergodic.

To minimize the influence of the crystallite edges, we have calculated the majority of quantities with the space damping factor

$$Q_{i,j,\nu} = \exp(-\lambda R_{i,j,\nu}^2) , \tag{5.4}$$

where $R_{i,j,\nu} = 0$ corresponds to the center of the crystallite and λ has been chosen so that the two-unit-cell-thick ring close to the edge contributes only 8% to the total information. This "trick" involves a finite-wave-vector resolution and allows one to calculate quantities for any wave vector k. In contrast, the periodic boundary conditions without $Q_{i,j,\nu}$ would allow one to find averages only for discrete wave vectors.

VI. RESULTS FOR RDP AND ADP MODELS

A. Order parameters

The moduli of the order parameters are defined as

$$\eta_{\mathrm{Rb}} = \left| \left\langle \frac{1}{N} \sum_{i,j,\nu} e_\nu(\Gamma_3) u_{i,j,\nu}(t) Q_{i,j,\nu} \right\rangle_\tau \right| \tag{6.1}$$

for the paraelectric-ferroelectric phase transition, and

$$\eta_{\mathrm{ND}} = \left| \left\langle \frac{1}{N} \sum_{i,j,\nu} e_\nu(Z_2+Z_3, s) u_{i,j,\nu}(t) \times e^{-2\pi i k R_{i,j,\nu}} Q_{i,j,\nu} \right\rangle_\tau \right| \tag{6.2}$$

for the paraelectric-antiferroelectric phase transition. The symmetry of the crystal allows one to choose the polarization vectors related to the Γ_3 and Z_2+Z_3 irreducible representations as

$$e(\Gamma_3) = (1,-1,1,-1,-1,-1) , \tag{6.3}$$

and

$$\begin{aligned} e(Z_2+Z_3, 1) &= (1,1,0,0,0,0) , \\ e(Z_2+Z_3, 2) &= (0,0,1,1,0,0) , \end{aligned} \tag{6.4}$$

and $Q_{i,j,\nu}$ is a damping factor [see Eq. (5.4)]. The spontaneous polarization of the system is proportional to η_{Rb}. Conventionally, the order parameters are defined within one domain. Here, they are described over the whole region of the crystallite. Since the domains differ by their signs, η_{Rb} and η_{ND} can diminish considerably, when more than one domain occurs in the system.

To find the order parameters we proceeded as follows. The molecular-dynamic calculations were started from initial conditions leading to a paraelectric phase, where $\eta_{\mathrm{Rb}} = \eta_{\mathrm{ND}} = 0$. Then the system was slowly cooled down in the presence of external fields E_{Rb} or $E_{\mathrm{NDx}}, E_{\mathrm{NDy}}$, respectively, and only one domain was formed at low temperature. The results of the order-parameter calculation for these runs are shown in Fig. 3, curve 1. Now, removing the external fields and heating the system, the order parameters decrease; see curves 2 and 3. Two different heating rates established the transition temperatures to be $T_c = 0.005\,65$ and 0.00430 for the RDP and ADP systems, respectively. Although the values of $\omega_{k,s}$ for Γ_3 and Z_2+Z_3 are the same, the transition temperatures are different. This is caused by different contributions in the fourth-order term $V^{(4)}$. Indeed, in the RDP case all components of the polarization vector (6.3) contribute to $V^{(4)}$, while in the ADP case only proton components of Eq. (6.4) enter into $V^{(4)}$.

Slow cooling from paraelectric phases, Fig. 3, curve 4, leads to a structure with few domains. Fast cooling leads to the state with many small domains the size of a few lattice constants, but the structure within a domain is perfect. The order parameters η_{Rb} and η_{ND} do not depend on the averaging time $\langle \cdots \rangle_\tau$, Eq. (5.1).

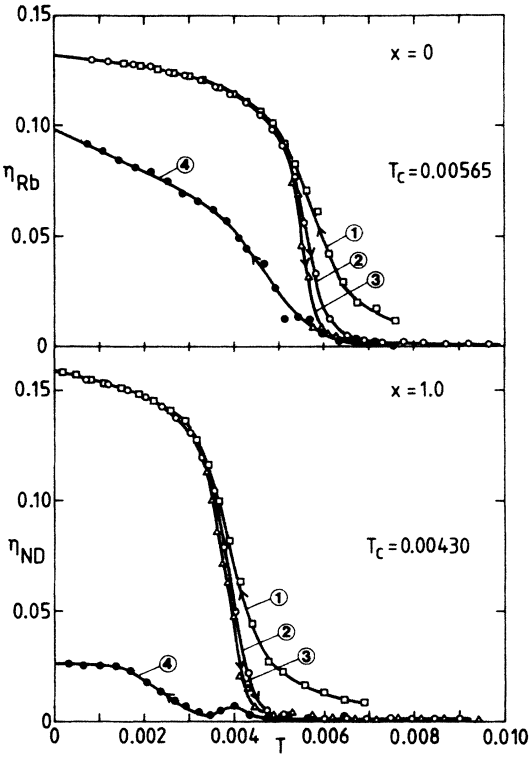

FIG. 3. Temperature behavior of the order parameters (6.1) and (6.2) of the RDP and ADP models taken with different external fields and different heating and cooling rates dT/dt. Curve 1, $E_{Rb}=0.001$ or $E_{NDx}=E_{NDy}=0.001$ and $dT/dt=-4\times10^{-6}$. Curves 2,3,4, $E_{Rb}=E_{NDx}=E_{NDy}=0$ and $dT/dt=4\times10^{-6}$, 2×10^{-6}, and -4×10^{-6}, respectively.

B. Average potential energy

The average potential energy $\langle V\rangle_\tau$ was calculated as a time average of formulas (3.1)—(3.5) and the results are shown in Fig. 4. During cooling from the paraelectric phase, the linear behavior is abandoned at the transition temperature T_c. In the multidomain system $\langle V\rangle_\tau$ has a higher potential energy than the relevant one-domain system, and the difference corresponds to domain-wall energies. Of course, domain walls disappear above the transition temperature.

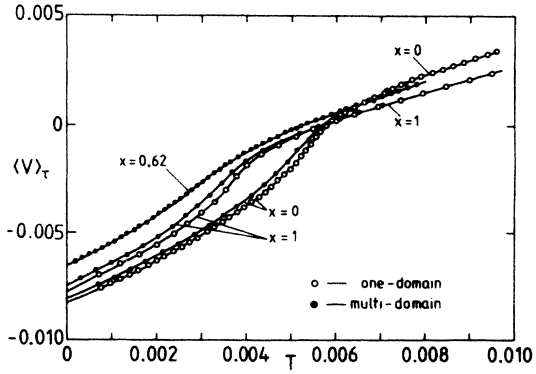

FIG. 4. Average potential energy $\langle V\rangle_\tau$, Eqs. (3.1)—(3.4), as a function of temperature for RDP and ADP models, and a glass model with concentration $x=0.62$.

VII. RESULTS FOR THE MODEL OF GLASS RADP

A. Phase diagram

Each point of the phase boundary in the calculated phase diagram of the mixed system, Fig. 5, was established by extrapolating the behavior of the order parameters η_{Rb} or η_{ND}, Eqs. (6.1) and (6.2), to zero. The zero-field behavior was found from extrapolation of two cooling runs with different external fields. Obviously, η_{Rb} and η_{ND} are nonzero close to $x=0$ and $x=1$, respectively. In the range of concentration $x\simeq0.4$—0.7, the magnitudes of the order parameters η_{Rb} and η_{ND} are negligible.

B. Average potential energy of glass

In Fig. 4 the average potential energy $\langle V\rangle_\tau$, Eqs. (3.1)—(3.5), for a glass of concentration $x=0.62$, is shown. The influence of initial conditions on $\langle V\rangle_\tau$ behavior is negligible. The average potential energy of the glass is higher than those of the pure crystals, even if the crystal possesses few domain walls. This means that the destruction of long-range order in the glass costs some energy.

C. Glass order parameter

We define the glass order parameter of our model as

$$\eta_\tau=\frac{1}{N}\sum_{i,j,\nu}(\langle u_{i,j,\nu}\rangle_\tau)^2\,, \tag{7.1}$$

where the summation goes over all particles. η_τ does not vanish when at least a few particles remain in positive or negative positions during time τ. We have checked that η_τ is independent of the initial conditions, which is natural for such an integrated quantity and such a large a crystallite.

The analogue of the Edwards-Anderson order parameter for an Ising spin system[23,24] will be $\lim_{\tau\to\infty}\eta_\tau$. The freezing temperature of a glass is usually defined by extra-

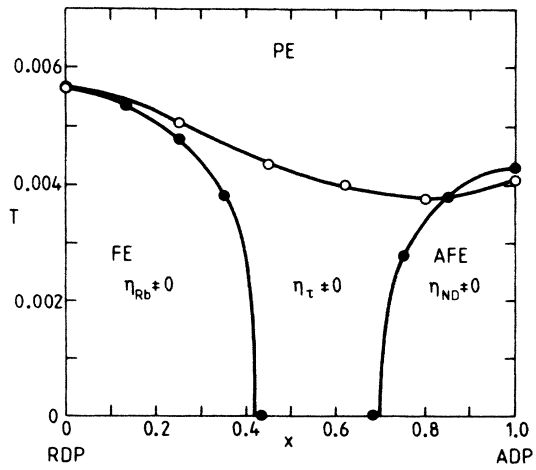

FIG. 5. Phase diagram of the RADP model. The freezing-temperature line for the time average with $\tau=200\tau_0$ is also indicated.

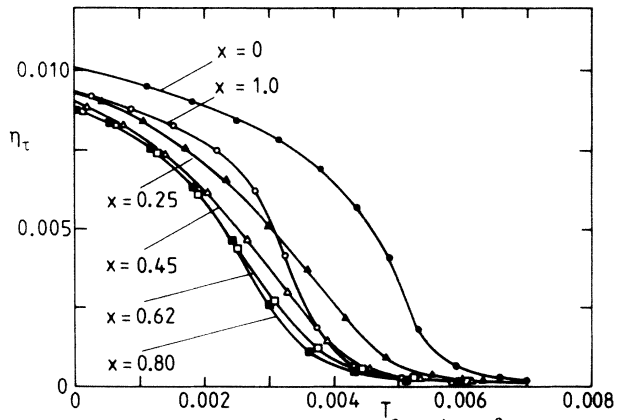

FIG. 6. Glass order parameter as a function of temperature calculated with the time average $\tau=200\tau_0$, and for several concentrations x, including RDP and ADP.

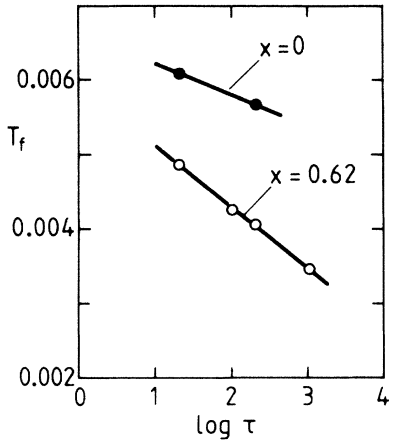

FIG. 8. Freezing temperature T_f as a function of $\log\tau$ for concentration $x=0.62$ and RDP model in a multidomain state.

polating the temperature-dependent $\eta_{\tau=\infty}$ curve to zero. The spectrum of the relaxation times of a glass is rather broad and the limit $\tau\to\infty$ in the definition of the Edwards-Anderson order parameter should exceed the longest relaxation time of the system. This limit is not accessible by a computer simulation. For a finite averaging time τ, the average will not "see" these relaxation times that are longer than τ and, therefore, the freezing temperature depends on averaging time τ.

The following calculations have been performed. First, for a few concentrations x the glass order parameter was found during slow cooling from the paraelectric state with an averaging time $\tau=200\tau_0$, and the results are shown in Fig. 6. Extrapolating η_τ to zero, the freezing temperature T_f was estimated as shown in the phase diagram, Fig. 5. For longer averaging times this freezing-temperature line will be placed lower. Second, for $x=0.62$ and several averaging times the glass order parameter was calculated as above, Fig. 7. In the intermediate temperature range, η_τ depends on the averaging time and this involves the τ dependence of the freezing temperature T_f. We found $T_f\sim\log\tau$ and these data are presented in Fig. 8, together with points T_f evaluated in the same manner for the RDP model. The glass order parameter of the pure system depends less on the averaging time τ because only the motion of particles close to a domain wall contribute to the changes of η_τ.

From these data one is, of course, not able to judge whether T_f goes to zero or not, when $\tau\to\infty$. However, at zero temperature the motion of the classical system stops and the glass order parameter has a finite value and is independent on the averaging time, Fig. 7.

Using the orthogonality properties of the polarization vectors $e_\nu(k,s)$ and Eq. (3.6), one finds

$$\eta_\tau=\sum_{k,s}|\langle\eta_{k,s}\rangle_\tau|^2 .$$

Each $\langle\eta_{k,s}\rangle_\tau$ has the symmetry of one of the components of the irreducible representation of the high-symmetry space group $I\bar{4}2d$ of the crystal, and all irreducible representations contribute to η_τ in the same way. The glass order parameter η_τ has the symmetry of the unit representation. Each $\langle\eta_{k,s}\rangle_\tau$ separately would define an order parameter of the normal phase transition, and then the sign of $\langle\eta_{k,s}\rangle_\tau$ would select the low-symmetry domains.

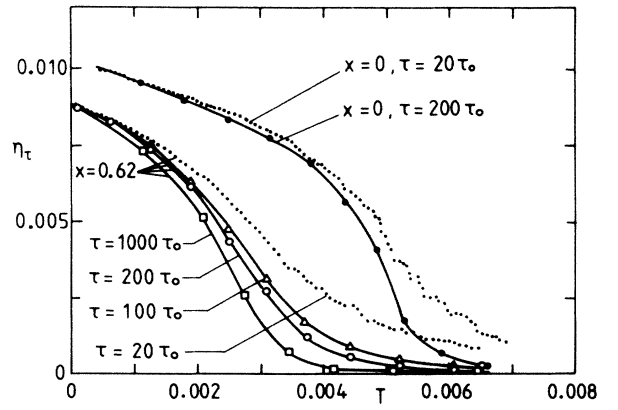

FIG. 7. Glass order parameter for a glass model with a concentration $x=0.62$ and RDP model in multidomain state, as a function of temperature for several averaging times τ.

D. Diffuse scattering function

Let us introduce the Fourier transform of the proton density of the crystal as

$$\epsilon(k,t)=\frac{1}{N}\sum_{i,j}\sum_{\nu=1}^{4}\exp\{-2\pi ik[R_{i,j,\nu}+u_{i,j,\nu}(t)]\}Q_{i,j,\nu} . \tag{7.2}$$

First, we define the diffuse scattering function as a time-independent correlation function,

$$F(k)=\langle\epsilon^*(k,t)\epsilon(k,t)\rangle_\tau , \tag{7.3}$$

where only the time average is applied. This function contains Bragg reflections and usually not intense diffuse scattering. Thus, for practical reasons it is better to split (7.2) into

$$\epsilon(k,t)=\langle\epsilon(k,t)\rangle_\tau+\rho(k,t)$$

and calculate the two terms of $F(k)$ separately, and then

$$F(k)=\langle\epsilon^*(k,t)\rangle_\tau\langle\epsilon(k,t)\rangle_\tau+\langle\rho^*(k,t)\rho(k,t)\rangle_\tau . \quad (7.4)$$

The term $|\langle\epsilon(k,t)\rangle_\tau|^2$ describes the Bragg reflections. We have checked that the Bragg peaks at the Γ point (22) occur for all phases and the superlattice reflection at the Z point (21) appears in the region of the antiferroelectric phase, indicated in the phase diagram in Fig. 5. The diffuse scattering was extensively studied for a glass model with concentration $x=0.62$, the same as in our experiment.[8] To find whether the time average is adequate we have started the calculations from initial conditions at about $T=0.003\,50$, cooled down to $T=0.001\,12$, and equilibrated. Then the data were collected in order to calculate, from (7.4), the diffuse scattering function as a time average over $\tau=2500\tau_0$. The $F(k)$ along two lines of reciprocal space are shown in Fig. 9. They indicate that rather complicated frozen modulation exists in the system. Then, the same system was allowed to evolve further during the next $\tau=2500\tau_0$, and the diffuse scattering functions, also shown in Fig. 9, were again calculated. The general peaked features of both curves remain. Consequently, a rather long averaging time does not lead to results which are representative for the experimental observations.

The comparison of two diffuse scattering functions obtained using the same cooling and equilibrating procedure as above, the same distribution of rubidium and ammonium, and the same averaging time $\tau=2500\tau_0$, but two different initial conditions, is shown in Fig. 10. Both curves are entirely different. Thus, applying two different initial conditions, the system has arrived at two different local minima, having approximately the same energy, but completely different displacement configurations. It is worth noticing how precisely the diffuse scattering function can differentiate different local minima.

The above result proves that, at low temperatures below

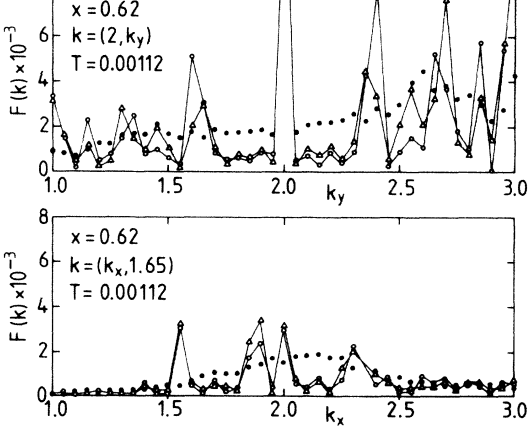

FIG. 9. Time-averaged diffuse scattering functions $F(k)$ at $T=0.001\,12$ and for two lines in the reciprocal space. The open dots indicate $F(k)$ averaged over $\tau=2500\tau_0$; open triangles denote $F(k)$ averaged over the next $\tau=2500\tau_0$. The solid dots denote the configurational average $\{F(k)\}_C$ over $C=80$ configurations.

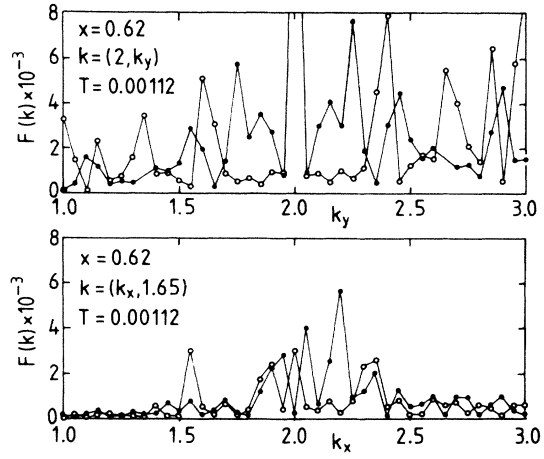

FIG. 10. Time-averaged diffuse scattering functions $F(k)$ at $T=0.001\,12$ and for two lines in the reciprocal space. The open and filled circles indicate $F(k)$ averaged over $\tau=2500\tau_0$, but started with different initial conditions, respectively.

T_f, the time average (5.1) and the configurational average (5.2) do not give the same results; therefore, the system is approximately nonergodic, Eq. (5.3), at least during the observation time over which the system could be studied by the molecular-dynamic method. This is not a long time in comparison to the times facilitated by some experimental techniques. If one observed the system for longer times, then T_f would diminish and the nonergodic effects would show up at lower temperatures.

At elevated temperatures, where the glass order parameter vanishes and the system becomes ergodic, the time average (5.1) should be equivalent to the configurational average (5.2). Indeed, Fig. 11 shows two results for the diffuse scattering function. In the first case we have applied one initial condition and found $F(k)$ averaged over $\tau=2500\tau_0$. In the second, we have used $C=80$ initial

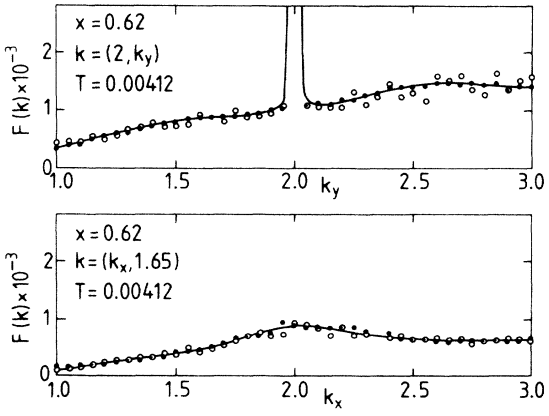

FIG. 11. Time $\tau=2500\tau_0$ (open dots) and configurational $C=80$ (solid dots) averages of diffuse scattering functions at $T=0.004\,12$ close to the freezing temperature, along two lines of reciprocal space. The time average for each $C=80$ configuration was $\tau=100\tau_0$.

conditions and calculated $\{F(k)\}_C$ with $\tau=100\tau_0$ in each run. The results are almost the same. The particular (but random) distribution of rubidium and ammonium prove to be not essential for the results.

To obtain a physically representative result for a macroscopic sample, one should average over many local minima, or, in other words, should calculate the configurational average (5.2) by applying many different, randomly chosen initial conditions. In this work the configurational average of the diffuse scattering function has always been calculated for $C=80$ configurations. Each particular run for these 80 configurations started from a given temperature, but not lower than $T=0.003\,50$, was cooled if necessary, and then equilibrated. The $F(k)$ function was averaged over $\tau=100\tau_0$, which was good enough, recalling the rather weak time behavior of the diffuse scattering function. The "observation" time $\tau=100\tau_0$ is compatible with a typical energy resolution $\Delta\omega\sim 2\pi/\tau$ of a neutron spectrometer, Fig. 9. The configurational averages at $T=0.001\,12$ indicated in Figs. 9 and 10 give smooth curves similar to the experimental observations.

The inelastic-neutron-scattering experiment performed on the single crystal $Rb_{0.38}(ND_4)_{0.62}D_2PO_4$ revealed elastic diffuse streaks along the high-symmetry direction $\langle 100\rangle$.[8] The most intense diffuse streaks occur around the (200), (240), and (150) reciprocal-lattice points, and in our model system we observe the diffuse streaks around the same points. We have, however, intensively studied only the diffuse scattering around the Γ point (22) along the [01] directions and perpendicular to it. The results, namely the configurational averages (5.2) with $C=80$ calculated as described above, are shown in Figs. 12 and 13. Figure 12 shows the diffuse scattering along the [01] direction. At the lowest temperature, $T=0.001\,12$, the diffuse streaks have a maximum at $0.65a^*$ from the Γ point (22), where $a^*=2\pi/a_0$. At elevated temperatures the diffuse peaks disappear.

The distribution of the diffuse streaks perpendicular to the [01] direction and $0.65a^*$ away from the Γ point are shown in Fig. 13. At low temperatures, $T=0.001\,12$, the distribution of $\{F(k)\}_C$ has a maximum around the high-symmetry line, and it broadens at elevated temperatures. It is instructive to draw its full width at half maximum (FWHM) as a function of temperature. The FWHM was defined at half-height from the "background," and the latter was taken as a straight line joining the points of $\{F(k)\}_C$ at $k_x=1$ and $k_x=3$. The FWHM of the distribution centered around $k=(2.0,1.35)$ and also around $k=(2.0,1.65)$ are shown in Fig. 14. Increasing the temperature, the widths remain constant up to $T=0.002\,75$ and then increase. The width for $k=(2.0,1.65)$ is larger than that of $k=(2.0,1.35)$ because the lowest dispersion curve $\omega_{k,s}$ has a shallower valley along the [01] direction at $k=0.35a^*$, which corresponds to $k=(2.0,1.65)$, than it does at $k=0.65a^*$. As mentioned in Sec. III, better results may be obtained only by introducing the acoustic branch. The increase of the FWHM of the diffuse streak, Fig. 14, has been already observed experimentally by Cowley *et al.*[7] and by us.[8] The change in slope of the FWHM occurs at temperatures

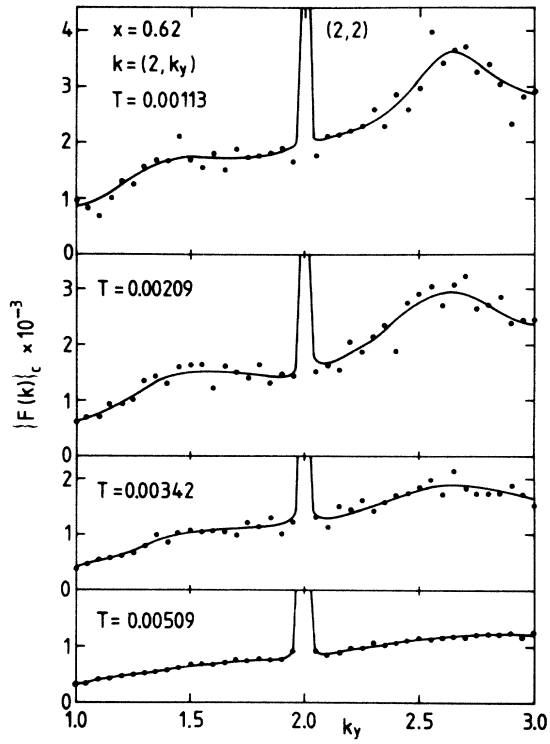

FIG. 12. Diffuse scattering functions $\{F(k)\}_C$ along the diffuse streaks close to the (22) Γ point for several temperatures, obtained as an average over $C=80$ configurations. The time average for each configuration was $\tau=100\tau_0$.

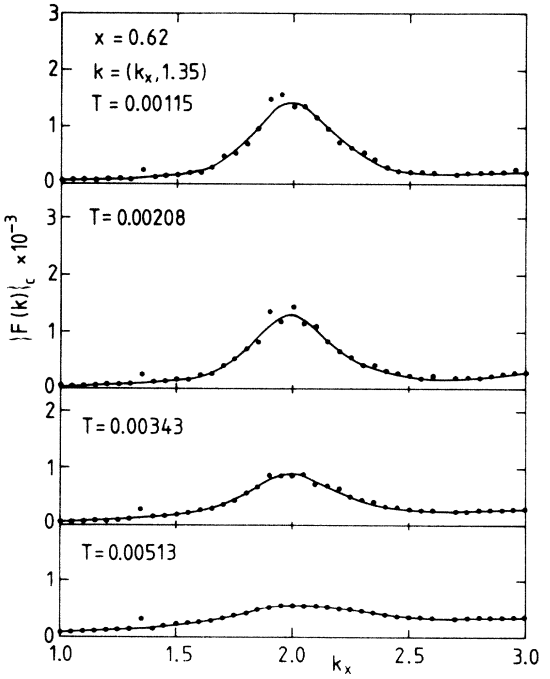

FIG. 13. Diffuse scattering functions $\{F(k)\}_C$ perpendicular to the diffuse streaks around its maximum at $k=(2.0,1.35)$ for several temperatures obtained as an average over $C=80$ configurations. The time average for each of $C=80$ configurations was $\tau=100\tau_0$.

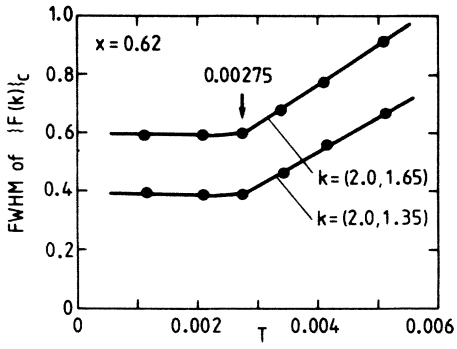

FIG. 14. Full width at half maximum of the diffuse streak distribution at two wave vectors, and perpendicular to [01] direction as a function of temperature.

where the glass order parameter, Fig. 7, is approximately equal to half of its maximum. At that point the correlation between even well-bounded particles starts to deteriorate.

A single run made at $T=0.001\,12$ for a concentration $x=0.45$ shows that the maximum of the diffuse streak along the [01] direction occurs at $0.35a^*$, and this shift towards the Γ point is compatible with the shift of the minimum of the average $\omega_{k,s}$ for the mixture $x=0.45$, see Sec. III.

E. Dynamical structure factor

The dynamical structure factor for the proton subsystem is defined as a Fourier transform of the time-dependent correlation function

$$S(k,\omega)=\frac{1}{2\pi}\int_{-\infty}^{\infty} dt\langle\epsilon^*(k,0)\epsilon(k,t)\rangle_\tau \times \exp[-(t/\gamma)^2]e^{i\omega t}, \quad (7.5)$$

where $\epsilon(k,t)$ is given by Eq. (7.2). We have included in the transformation the Gaussian damping factor $\exp[-(t/\gamma)^2]$, which is necessary when calculating long-time correlations and which plays the same role as a Gaussian resolution function in the instrument which measures $S(k,\omega)$. The "experimental" energy resolution is then $\Delta\omega=(4/\gamma)(\ln 2)^{1/2}$. The dynamical structure factor also has some wave-vector resolution, defined by the damping factor $Q_{i,j,\nu}$ [Eq. (5.4)].

The $S(k,\omega)$ may contain elastic scattering. Therefore, as in Sec. VII D, it is better to decouple

$$\epsilon(k,t)=\langle\epsilon(k,t)\rangle_\tau+\rho(k,t),$$

and to calculate the elastic (el) and inelastic (ie) parts (within a given energy resolution) separately:

$$S(k,\omega)=S^{\mathrm{el}}(k,\omega)+S^{\mathrm{ie}}(k,\omega), \quad (7.6)$$

$$S^{\mathrm{el}}(k,\omega)=\langle\epsilon^*(k,0)\rangle_\tau\langle\epsilon(k,t)\rangle_\tau\frac{\gamma}{2\pi} \times \exp[-(\gamma^2\omega^2)/4], \quad (7.7)$$

$$S^{\mathrm{ie}}(k,\omega)=\frac{1}{2\pi}\int_{-\infty}^{\infty} dt\langle\rho^*(k,0)\rho(k,t)\rangle_\tau \times \exp[-(t/\gamma)^2]e^{i\omega t}. \quad (7.8)$$

For a perfect resolution, $\gamma\to\infty$ and the elastic part tends to $|\langle\epsilon(k,0)\rangle_\tau|^2\delta(\omega)$.

At low temperatures the model glass system goes to one of the local minima with not only specific displacements but also specific occupation of the dynamical modes. In effect, the intensities of the dynamical structure factor depend upon the initial conditions. It has been proved that the studied crystallite is too small to possess an occupation of modes required by the equilibrium condition. However, by changing the initial conditions different local minima and occupation of modes can be reached, and the configurational average of $\{S(k,\omega)\}_C$, Eq. (5.2), can be calculated. This average should be compared with experimental data. We have used $C=80$ configurations. In each run such initial conditions have been taken, which lead to a desired temperature, but not lower than $T=0.003\,50$, and then the system, if necessary, was cooled and equilibrated during $\tau=100\tau_0$. For each run the information was collected during $100\tau_0$, and the time-dependent correlation function $\langle\rho^*(k,0)\rho(k,t)\rangle_\tau$ was cal-

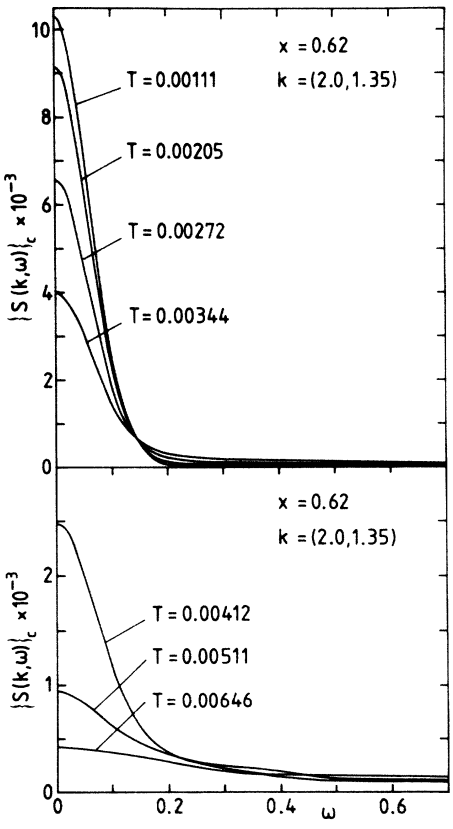

FIG. 15. Dynamical structure factor $\{S(k,\omega)\}_C$ for $k=(2.0,1.35)$ as a function of temperature. The time average for each of $C=80$ configurations was $\tau=50\tau_0$. The energy resolution was $\Delta\omega=0.141$.

culated for a time interval $t=(0\div 50)\tau_0$ and averaged over $\tau=50\tau_0$. The energy resolution is $\Delta\omega=0.141$.

At low temperatures the dynamical structure factor $\{S(k,\omega)\}_C$ for a glass model of concentration $x=0.62$ and wave vector $k=(2.0,1.35)$, Fig. 15, consists of an elastic peak and a long, slowly decaying inelastic background. No inelastic peaks have been observed up to $\omega=5$. The elastic peak arises as a result of static disorder. In the model system of RDP or ADP the intensity of the elastic contribution would be strongly reduced because the coherence of the elastic scattering is not broken by static displacements. The elastic peak for the glass model decreases with increasing temperature. Simultaneously, the inelastic background increases. This means that the static character of the displacements changes to the dynamical behavior with a characteristic time the order of the inverse energy resolution.

It is worthwhile to indicate the contribution of the elastic and inelastic parts to the dynamical structure factor at $\omega=0$. Figure 16 gives these contributions as a function of temperature. The elastic contribution decreases with temperature, while the "elastic" contribution from the inelastic part shows a critical behavior around $T=0.003\,50$. One should remember, however, that this separation into elastic and inelastic parts is rather arbitrary and depends on the energy resolution $\Delta\omega$.

The full width at half maximum of the dynamical structure factor $\{S(k,\omega)\}_C$ as a function of temperature is shown in Fig. 17. At low temperatures the FWHM is equal to the resolution and it rises above it around $T=0.003\,00$. This means that at this temperature there appears a relaxation time shorter than the "resolution" time $2\pi/\Delta\omega\simeq 45\tau_0$. This behavior is in full agreement with the experimental observations[8] and theoretical description.[25]

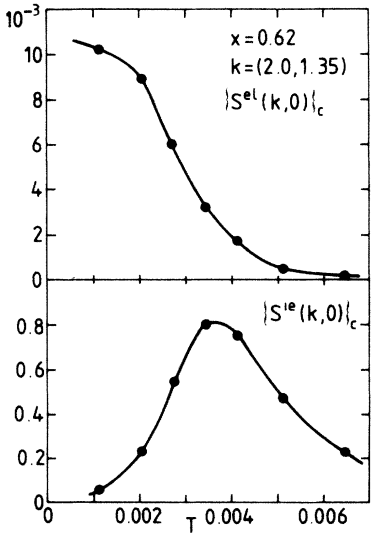

FIG. 16. Amplitudes of elastic and inelastic parts of dynamical structure factor at $\omega=0$ for $k=(2.0,1.35)$ as a function of temperature. The time average for each of $C=80$ configurations was $\tau=50\tau_0$. The energy resolution was $\Delta\omega=0.141$.

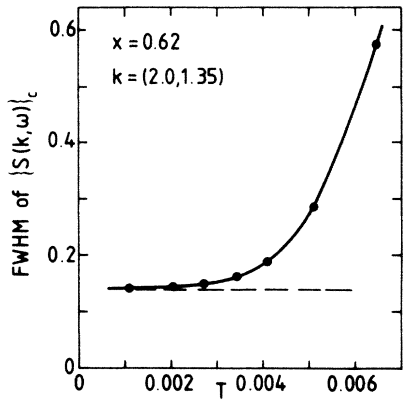

FIG. 17. Full width at half maximum in ω of the dynamical structure factor for $k=(2.0,1.35)$ as a function of temperature. The time average for each of $C=80$ configurations was $\tau=50\tau_0$. The energy resolution was $\Delta\omega=0.141$ (dashed line).

VIII. DISCUSSION

Our calculations have shown that the main features of the crystal statics and dynamics of $Rb_{1-x}(ND_4)_xD_2PO_4$ can be understood on the basis of a two-dimensional model. The model studied has a freezing temperature T_f to a glassy state. Above T_f the relaxation in the system is so fast that the time average, over times available by computer simulation, is sufficient to produce representative physical results. Below T_f the model system goes to local minima. To arrive at different minima, the history of the sample must be different, and this can be achieved by applying, for example, different initial conditions. The integral quantities, such as average potential energy and glass order parameter, show negligible dependence of the local minima. Two local minima differ by the pattern of displacements, even if the underlying distribution of rubidium and ammonium, which produces a kind of random field, remains the same. The distribution of the diffuse scattering, which is the Fourier transform of the displacement correlation pattern, changes significantly from one local minimum to another.

The calculated diffuse streaks resemble unevolved satellites, occurring in the incommensurate structures. There, the phase transition to an incommensurate structure arises as a result of the softening of a displacive or occupational mode, or a mixed mode of both. In the glassy state the situation is somewhat similar. The diffuse streak occurs at the wave vectors where the average dispersion curve $\omega_{k,s}$ has a minimum. Sharp satellites or superreflections cannot arise, however, because the long-range order in glass is destroyed by the random field of the underlying distribution of rubidium and ammonium. Perhaps it is worth mentioning that a mixed crystal can form a glassy state only when the "soft mode" is of occupational type. For a displacive mode the barriers between the local minima disappear and the glassy state will not appear.

The freezing temperature T_f of the model depends on the averaging time, and for this time the system is approximately ergodic above T_f and approximately nonergodic below T_f. In such nonergodic states there exist re-

laxation times which are longer than the times of observation. The freezing temperature decreases if longer averaging times are applied. However, by the use of the molecular-dynamic method one is not able to answer the question of whether the freezing temperature goes to zero if the averaging time tends to infinity. On the other hand, a short time ($10^2\tau_0$) is sufficient for the description of the scattering functions, which should be calculated with the aim of attaining the configurational average. Each run of the configurational average, starting from rather arbitrary initial conditions, needs to be equilibrated before use. Because of the obvious practical reasons, the equilibration time cannot be too long, and we have used the same time as the average time for a given quantity. Therefore, the system could still relax. The corrections, however, should not be large, since the relaxation times which still drive the system toward a local minimum are not "seen" by the calculated averages.

ACKNOWLEDGMENTS

The authors wish to thank T. Springer, K. H. Michel, J. Villain, E. Courtens, H. Müller-Krumbhaar, and K. H. Fisher for valuable comments, G. Groten for supplying some subroutine programs, and D. Bartel, H. W. Homrighausen, and K. Wingerath for advice during the construction of the program. One of us (K.P.) would like to express his thanks to the staff of Institut für Festkörperforschung und Zentralinstitut für Angewandte Mathematik, Kernforschungsanlage, Jülich, for their hospitality and assistance.

*Permanent address: Institute of Nuclear Physics, ulica Radzikowskiego 152, PL-31-342 Krakow, Poland.

[1]E. Courtens, Helv. Phys. Acta **56**, 705 (1983).
[2]S. Iida and H. Terauchi, J. Phys. Soc. Jpn. **52**, 4044 (1983).
[3]E. Courtens, Phys. Rev. Lett. **52**, 69 (1984).
[4]E. Courtens, T. E. Rosenbaum, S. E. Nagler, and P. M. Horn, Phys. Rev. B **29**, 515 (1984).
[5]J. Slak, R. Kind, R. Blinc, E. Courtens, and S. Zumer, Phys. Rev. B **30**, 85 (1984).
[6]E. Courtens and H. Vogt, J. Chem. Phys. (Paris) **82**, 317 (1985).
[7]R. A. Cowley, T. Ryan, and E. Courtens, J. Phys. C **18**, 2793 (1985).
[8]H. Grimm, K. Parlinski, W. Schweika, E. Courtens, and H. Arend, Phys. Rev. B (to be published).
[9]S. Hayase, T. Futamura, H. Sakashita, and H. Terauchi, J. Phys. Soc. Jpn. **54**, 812 (1985).
[10]K. H. Michel and J. M. Rowe, Phys. Rev. B **22**, 1417 (1980).
[11]D. G. Bounds, M. L. Klein, I. R. McDonald, and Y. Ozal, Mol. Phys. **47**, 629 (1982).
[12]P. Prelovsek and R. Blinc, J. Phys. C **15**, L985 (1982).
[13]E. Matsushita and T. Matsubara, Prog. Theor. Phys. **71**, 235 (1984).
[14]E. Matsushita and T. Matsubara, J. Phys. Soc. Jpn. **54**, 1161 (1985).
[15]E. Matsushita and T. Matsubara, J. Phys. Soc. Jpn. **54**, 2032 (1985).
[16]G. S. Pawley and J. E. Tibballs, Ferroelectric Lett. **44**, 33 (1982).
[17]H. H. Hahn, in *Kinetics of Aggregation and Gelation,* edited by F. Family and D. P. Landau (Elsevier, Amsterdam, 1984), p. 235.
[18]K. Gesi, K. Ozawa, T. Osaka, and Y. Makita, J. Phys. Soc. Jpn. **52**, 2538 (1983).
[19]S. Suzuki, K. Arai, M. Sumita, and Y. Makita, J. Phys. Soc. Jpn. **52**, 2394 (1983).
[20]O. V. Kovalev, *Irreducible Representations of the Space Groups* (Gordon and Breach, New York, 1965).
[21]H. Konwent and J. Lorenc, Phys. Status Solidi B **88**, 747 (1978).
[22]K. Parlinski, Z. Phys. B **58**, 245 (1985).
[23]S. F. Edwards and P. W. Anderson, J. Phys. F **5**, 965 (1975).
[24]K. H. Fisher, Phys. Status Solidi B **116**, 357 (1983).
[25]H. Sompolinsky and A. Zippelius, Phys. Rev. B **25**, 6860 (1982).